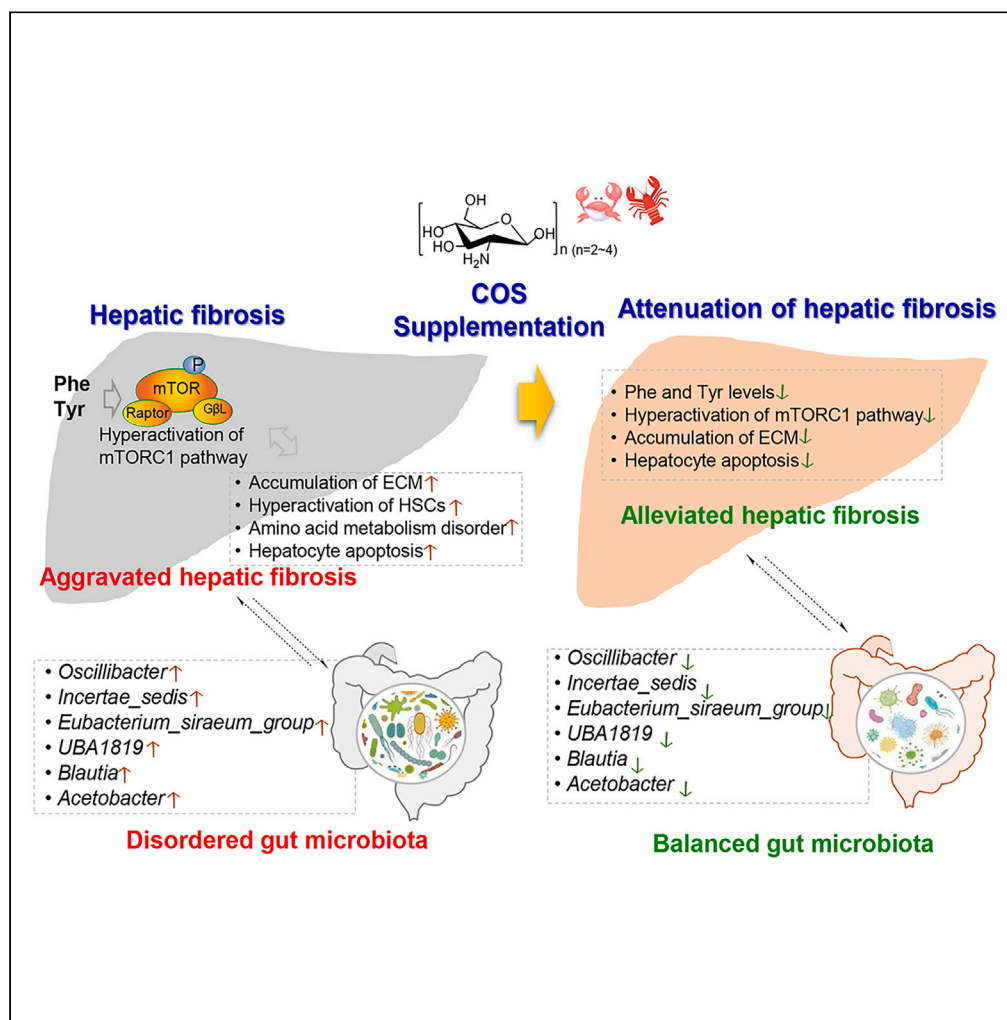# iScience

Article

Aggravated hepatic fibrosis induced by phenylalanine and tyrosine was ameliorated by chitooligosaccharides supplementation

Peng Liu, Heng Li, Hongyu Xu, Jinsong Gong, Min Jiang, Zhenghong Xu, Jinsong Shi

liheng@jiangnan.edu.cn

Highlights

COS reduces Phe and Tyr levels in the serum of mice with hepatic fibrosis

Phe and Tyr exacerbate hepatic fibrosis symptoms and gut microflora dysbiosis

COS ameliorates hepatic fibrosis with the regulation of Phe and Tyr metabolism

iScience

Article

Aggravated hepatic fibrosis induced by phenylalanine and tyrosine was ameliorated by chitooligosaccharides supplementation

Peng Liu,[1,2] Heng Li,[1,4,*] Hongyu Xu,[3] Jinsong Gong,[1] Min Jiang,[1] Zhenghong Xu,[3] and Jinsong Shi[1]

SUMMARY

Hepatic fibrosis is a classic pathological manifestation of metabolic chronic hepatopathy. The pathological process might either gradually deteriorate into cirrhosis and ultimately liver cancer with inappropriate nutrition supply, or be slowed down by several multifunctional nutrients, alternatively. Herein, we found diet with excessive phenylalanine (Phe) and tyrosine (Tyr) exacerbated hepatic fibrosis symptoms of liver dysfunction and gut microflora dysbiosis in mice. Chitooligosaccharides (COS) could ameliorate hepatic fibrosis with the regulation of amino acid metabolism by downregulating the mTORC1 pathway, especially that of Phe and Tyr, and also with the alleviation of the dysbiosis of gut microbiota, simultaneously. Conclusively, this work presents new insight into the role of Phe and Tyr in the pathologic process of hepatic fibrosis, while revealing the effectiveness and molecular mechanism of COS in improving hepatic fibrosis from the perspective of metabolites.

INTRODUCTION

Hepatic fibrosis is characterized by excessive accumulation of extracellular matrix (ECM) in liver, a precursor pathology to cirrhosis, which could further cause an increase in mortality.[1,2] Activation of myofibroblasts from vitamin A-storing quiescent hepatic stellate cells (HSCs) is a critical driver in the progression of hepatic fibrosis as these cells become the primary source of ECM.[3] Clinical and experimental hepatic fibrosis was reportedly regressed when the causative agent was eliminated, such as activated HSC and fibrous scar.[4] However, the mechanisms underlying the occurrence and reversibility of hepatic fibrosis are still unclear, including those underlying HSC activation, cellular sources of ECM, and the pathway of fibrosis regression. Continued efforts over the past few decades have greatly increased the knowledge of the molecular mechanisms of hepatic fibrosis.[5] It is noteworthy that abnormal metabolism can induce negative feedback on cellular responses in the liver.[6] For instance, overaccumulation of lipids in hepatocytes could drive HSC activation and further induce carbohydrate metabolism dysfunction.[7,8] Moreover, converging evidence from recent epidemiological studies has revealed that a disorder of amino acid metabolism supports remodeling of the ECM and breakdown of immune homeostasis, which is related to the pathogenesis of hepatic fibrosis.[9–11] Clinical and related basic studies are constantly providing new information on the puzzle of liver injury, revealing that increased levels of aromatic amino acids (AAAs) and decreased levels of branched-chain amino acids are an index of the degree of severity and prognosis of hepatic fibrosis.[12] Concurrently, high levels of AAAs continue to exhibit a pathophysiological effect in hepatopathy, including hepatic fibrosis and liver cancer, for example, Phe and its metabolites can induce liver steatosis.[13] Additionally, imbalance of amino acid metabolism homeostasis has been revealed closely relating to alterations in gut microbiota.[14] Liver could affect intestinal microbial communities through the hepato-intestinal axis, in which the gut microbiota acts as a key part of this bidirectional communication. Therefore, the control of microbial communities is critical for maintaining homeostasis. As an effector of amino acid, mammalian target of rapamycin complex 1 (mTORC1) has a double-edged role: on the one hand, it can integrate diverse signals to maintain homeostasis of cell metabolism,[15,16] while on the other hand, it can trigger hyperactivation of HSCs which serves as a therapeutic target to block the development of hepatic fibrosis.[17] However, the mechanism of these cascadic reactions caused by dysfunction of amino acid metabolism remains unclear.

Functional food not only provides basic nutrition but also possesses the ability of the regulating metabolism, and further affects liver function. Chitooligosaccharides (COS), typical amino-oligosaccharides, have been proved to possess the ability of hepatoprotection, reflected in inhibiting hepatoma progression, improving glucolipid metabolism disorder in fatty livers, and resisting oxidative stress in ethanol-induced acute hepatic injury.[18–20] In our previous study, COS significantly ameliorated toxicity and liver function in carbon tetrachloride (CCl$_4$)-induced hepatic fibrosis model.[21,22] However, little information is currently available on the metabolic modulation mechanism of COS in hepatopathy,

[1]Key Laboratory of Carbohydrate Chemistry and Biotechnology, Ministry of Education, School of Life Sciences and Health Engineering, Jiangnan University, Wuxi 214122, China
[2]Institute of Edible Fungi, Shanghai Academy of Agricultural Sciences, 1000 Jinqi Road, Shanghai 201403, China
[3]National Engineering Research Center for Cereal Fermentation and Food Biomanufacturing, Jiangnan University, Wuxi 214122, China
[4]Lead contact
*Correspondence: liheng@jiangnan.edu.cn
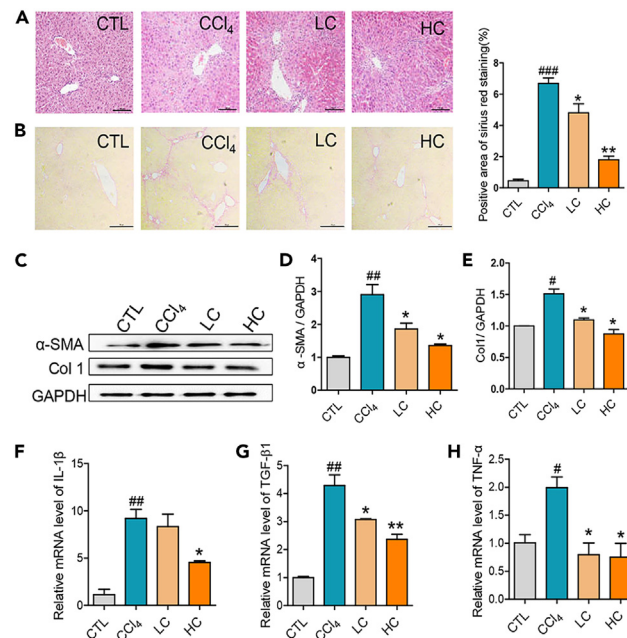https://doi.org/10.1016/j.isci.2023.107754

Figure 1. COS reversed the progression of CCl₄-induced hepatic fibrosis
(A–B) Hematoxylin-eosin and Sirius red staining of liver sections (n = 6).
(C) The protein levels of α-SMA and Col1 in liver tissues were analyzed by western blotting (n = 3).
(D and E) The grayscale of α-SMA and Col1.
(F–H) The mRNA levels of IL-1β, TGF-β1, and TNF-α (n = 6). All values are presented as means ± SEM. Significantly different (*p < 0.05, **p < 0.01) versus the CCl₄ group. Significantly different (#p < 0.05, ##p < 0.01 ###p < 0.001) versus the CTL group. Scale bar, 100 μm.

reflected in the evaluation of the metabolic pathway by assessment of key proteins or genes. This has limited our knowledge on the ameliorative effect of COS on liver disease. Moreover, direct empirical evidence is still lacking.

This study hypothesized that the anti-hepatic fibrosis efficacy of COS might be associated with the modulation of amino acid metabolism homeostasis, especially AAAs metabolism. Accordingly, from the perspective of metabolic profiling, the potential mechanism of COS in reversing hepatic fibrosis was explored in a CCl₄-induced mouse model of hepatic fibrosis by employing metabolomics. Furthermore, 16s RNA sequencing was performed to study the regulatory effect of COS based on gut-liver axis. These studies would contribute to further understanding of the underlying molecular mechanism of COS intervention in hepatic fibrosis and thus suggest a new anti-hepatic fibrosis strategy.

RESULTS

COS relieved the pathological process of hepatic fibrosis in mice

A preliminary evaluation of the amelioration of COS on hepatic fibrosis showed that hepatic lesions were apparent in CCl₄-treated mice, with the loss of parenchymal architecture and intense neutrophilic invasion. However, COS prevented hepatic lesions induced by CCl₄ (Figure 1A). Further, COS prevented fibrous collagen deposition and reduced the protein levels of α-smooth muscle actin (α-SMA) and Type I collagen (Col1) (Figures 1B–1E). Moreover, COS can inhibit the CCl₄-induced enhancement of the mRNA levels of interleukin (IL) -1β, tumor necrosis factor alpha (TNF-α), and transforming growth factor (TGF) -β1; especially, in the HC group, the mRNA levels of IL-1β, TGF-β1, and TNF-α, decreased by 50.7%, 45.0%, and 62.6%, respectively (Figures 1F–1H) (The primers used in qRT-PCR were shown in Table 1). Conclusively, COS could alleviate the pathological symptoms of mice with hepatic fibrosis.

Metabolite mapping for alleviation of hepatic fibrosis by COS supplementation

COS supplementation reduced Phe and Tyr levels in the serum of mice with hepatic fibrosis

The application of metabolomics in searching for hallmark metabolites in cells, organs, or excretions could reveal a pathway related to disease progression and prospectively explain the underlying mechanism. Therefore, serum metabolites were investigated by LC-MS/MS. There were 50 significantly different metabolites between heathy mice and COS-treated mice compared with those in hepatic fibrosis mice (p < 0.05) (Figure 2A). The intensities of 21 target metabolites were increased or decreased in mice with hepatic fibrosis but changed to basal levels in COS-treated mice (Figures 2B, S1, and S2). The levels of these metabolites were subjected to Ward's hierarchical clustering analysis to ascertain the accurate separation of the hepatic fibrosis mice and COS-treated mice (Figure 2B).

Table 1. Specific primers used for qRT-PCR analysis of gene expression

Species	Gene	Forward (5′–3′)	Reverse (5′–3′)
Mouse	TNF-α	ACCACGCTCTTCTGTCTA	TCCACTTGGTGGTTTGCT
Mouse	IL-1β	GCAACTGTTCCTGAACT	ATCTTTTGGGGTCCGTCA
Mouse	Caspaes 9	TCCTGGTACATCGAGACC	AAGTCCCTTTCGCAGAAA
Mouse	Caspase 3	CTGACTGGAAAGCCGAA	CGACCCGTCCTTTGAATT
Mouse	β-actin	GGCTGTATTCCCCTCCATC	CCAGTTGGTAACAATGCC
Human	α-SMA	CTATGAGGGCTATGCCTTG	GCTCAGCAGTAGTAACGA
Human	Col1a1	ATCAACCGGAGGAATTTC	CACCAGGACGACCAGGTTT
Human	Col4a1	CCAGGGGTCGGAGAGAA	GGTCCTGTGCCTATAACAAT
Human	TGF-β	GGCCAGATCCTGTCCAAG	GTGGGTTTCCACCATTAGC
Human	IL-1β	AGCTACGAATCTCCGACC	CGTTATCCCATGTGTCGAA
Human	TNF-α	GAGGCCAAGCCCTGGTAT	CGGGCCGATTGATCTCAGC
Human	Caspase 9	CTGTCTACGGCACAGATG	GGGACTCGTCTTCAGGGGA
Human	Caspase 3	AGAGGGGATCGTTGTAGA	ACAGTCCAGTTCTGTACCA
Human	IL-6	CCTGAACCTTCCAAAGAT	TTCACCAGGCAAGTCTCCT
Human	TAT	CTGGACTCGGGCAAATAT	GTCCTTAGCTTCTAGGGGT
Human	PAH	TTCCCAAGAACCATTCAA	GCGGTAGTTGTAGGCAATG
Human	TYR	GCAAAGCATACCATCAGC	GCAGTGCATCCATTGACAC
Human	β-actin	CATGTACGTTGCTATCCAG	CTCCTTAATGTCACGCACG

Furthermore, 10 metabolic pathways were found, seven of which were associated with amino acid metabolism and were the most influential metabolic pathways associated with COS treatment. In particular, the Phe, Tyr, and Tryptophan (Trp) biosynthesis pathway was very vital (Figure 2C). It is widely known that an enhancement in the blood levels of Phe and Tyr is associated with hepatopathy,[23,24] herein, this increase was indeed decreased by COS treatment. Detailed analysis showed that the intensities of Phe and Tyr in mice with hepatic fibrosis were increased, while the intensity of Trp remained relatively invariable (Figure S2). Consistently, HPLC analysis verified that COS treatment decreased the levels of Phe and Tyr in the serum of hepatic fibrosis mice (Figure 2D). Disorders of Phe metabolism are observed in the damaged liver, which is the main site of hydroxylation of Phe to Tyr and further degradation of Tyr.[25] Taken together, our results established the possible therapeutic strategy of using COS to ameliorate amino acid metabolic disorders in hepatic fibrosis, especially to abate the levels of Phe and Tyr.

COS treatment promotes the utilization of Phe and Tyr in injured hepatocytes in vitro

Given that liver damage caused by CCl_4 was accompanied by free radical generation, an in vitro study of L-02 cell injury induced by hydrogen peroxide (H_2O_2) was performed to further confirm whether COS drive the metabolism of Phe and Tyr. The metabolism of Phe and Tyr in damaged cells was lower than that in normal cells, but was enhanced by COS treatment (Figures S3A–S3C), consistent with the results obtained in vivo (Figure 2D). Moreover, the mRNA levels of key enzymes in the Phe and Tyr metabolic pathways were determined. In damaged cells, incubation with COS increased the mRNA levels of Phe hydroxylase (PAH), Tyr aminotransferase (TAT), and tyrosinase (TYR), which might be due to improvement in cell damage (Figures S3D–S3F) (The primers used in qRT-PCR were shown in Table 1). Summarily, the results verified that COS promoted the metabolism of Phe and Tyr, as biomarkers of hepatic fibrosis, which might be attributed to an increase in the expression level or activity of metabolic enzymes.

COS ameliorated the deterioration of liver dysfunction induced by Phe and Tyr

Imbalanced amino acid pools may continue to play a pathophysiological role in liver insufficiency.[26] In this study, the symptoms of liver injury induced by Phe and Tyr were apparent in CCl_4-treated mice, including inflammatory infiltration, vacuolization, and fat deposition, which were further aggravated by excessive Phe and Tyr supplement (Figures 3A–3C and S4). It is well known that pathological deposition of ECM is a fundamental feature of hepatic fibrosis. As the major ECM producer and hepatic fibrosis progression driver, activated HSCs are characterized by increased level of α-SMA. Compared with those in the CTL group, the collagen deposition, hydroxyproline (HYP), α-SMA and Col1 levels were increased upon Phe and Tyr treatment and CCl_4 challenge, while those in the Phe, Tyr, and CCl_4 combined treatment group were more enhanced than those in the single-CCl_4 treatment group (Figures 3D–3G). Compared with those in the CCl_4 group, the levels of collagen deposition, HYP, α-SMA, and Col1 in the Phe, Tyr, and CCl_4 combined treatment group were increased by 31.2%, 16.6%, 21.0%, and 15.6%, respectively. Coincidentally, the biochemical indicators reflecting liver function showed a consistent trend of change (Figure S5). Phe- and Tyr-induced hepatotoxicity was relieved by COS treatment (Figure 3). In summary, Phe and Tyr could cause the deterioration of liver function, which was blocked by COS treatment.
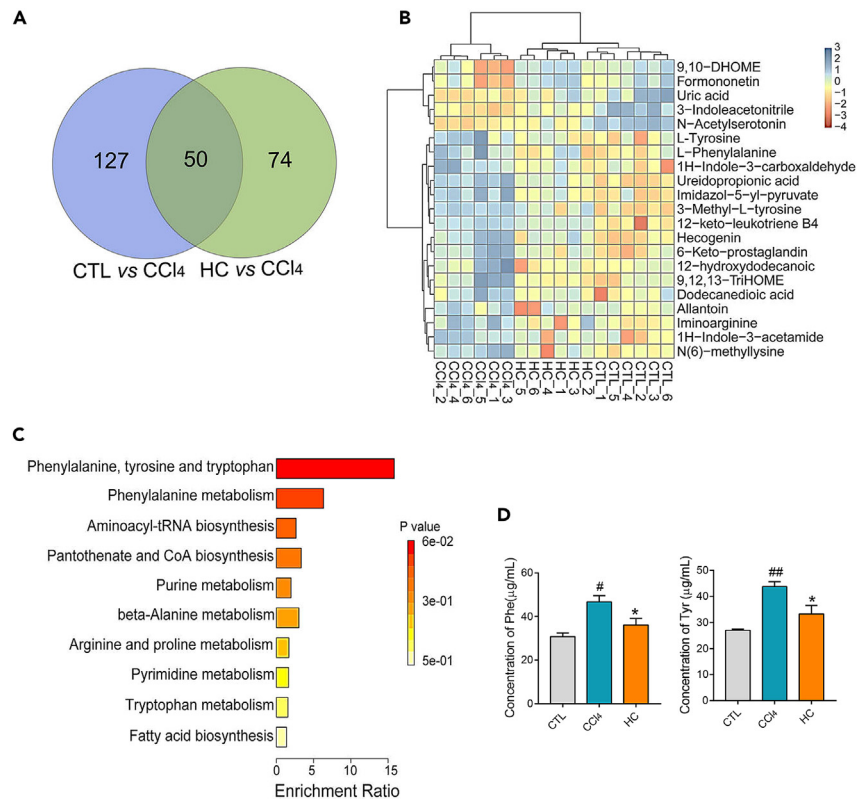
Figure 2. Identification of potential metabolites upon COS treatment

(A) Venn diagram showing the metabolites in the groups.

(B) The heatmap of 21 potential metabolites.

(C) Enrichment analysis combining function-related metabolites to determine consistent changes among related metabolites; the color and bar length indicate the p value and fold enrichment, respectively.

(D) The contents of Phe, Tyr, and Trp in serum samples were analyzed via HPLC (n = 3). All values are presented as means $\pm$ SEM. Significantly different (*p < 0.05) versus the CCl$_4$ group. Significantly different (#p < 0.05, ##p < 0.01) versus the CTL group. Not significantly different (ns p > 0.05).

Given that mTORC1 is located at the intersection of amino acid metabolism and hepatic fibrosis, it was reasonable to detect the status of the mTORC1 pathway.[27] The data exhibited that the phosphorylation levels of mTOR and 70-kDa ribosomal protein S6 kinase (p70 S6K1) were increased in mice challenged with CCl$_4$, indicating that the mTORC1 pathway was activated in mice with hepatic fibrosis, while it was inhibited by COS treatment (Figure S6). Furthermore, the mTORC1 pathway was consistently overactivated in the Phe, Tyr, and CCl$_4$ combined group compared with that in the single-CCl$_4$ treatment group, reflected by the enhancement of the levels of the downstream proteins of the mTORC1 pathway, including eIF4E and 4E-BP1 (Figure 4). The deterioration of the aforementioned pathological markers caused by Phe and Tyr was counteracted by the mTORC1 inhibitor RAP, suggesting that Phe and Tyr aggravated the liver dysfunction in mice with hepatic fibrosis by upregulating the mTORC1 pathway (Figures 3 and 4). Meanwhile, COS treatment palliated hepatic lesions, collagen deposition, and hyperactive mTORC1 pathway, which were abolished by the activator of mTORC1 (MHY1485, MHY) (Figure 4). Together, the data integrally illustrated that the severity of hepatic fibrosis was exacerbated by Phe and Tyr, but was decreased by COS treatment through the mTORC1 pathway.

Detailed exploration of the mechanism underlying the effect of COS supplementation on hepatic fibrosis

Repression of apoptosis in hepatocytes

Given the deteriorative effects of Phe and Tyr on hepatic fibrosis, it was of great value to investigate their influence on cell growth at the molecular level. The liver comprises multiple cell types, among which hepatocytes account for most of the volume of the liver and exercise main functions. Phe and Tyr indeed caused damage to L-02 cells, characterized by increased levels of IL-1β, TNF-α, caspase 3, and caspase 9 (Figure S7) (The primers used in qRT-PCR were shown in Table 1). Further, mitochondrial membrane potential was destroyed in the aa group (treatment with Phe and Tyr), while it was improved by COS (Figure 5A). The protein or gene levels of TGF-β1, mature IL-1β, TNF-α, caspase 9, and cleaved caspase 3 were all consistently enhanced after Phe and Tyr challenge, which were alleviated by COS treatment (Figures 5B–5F and S8). Moreover, Phe and Tyr stimulated hyperactivation of the mTORC1 pathway in L-02 cells, which was restored by COS treatment
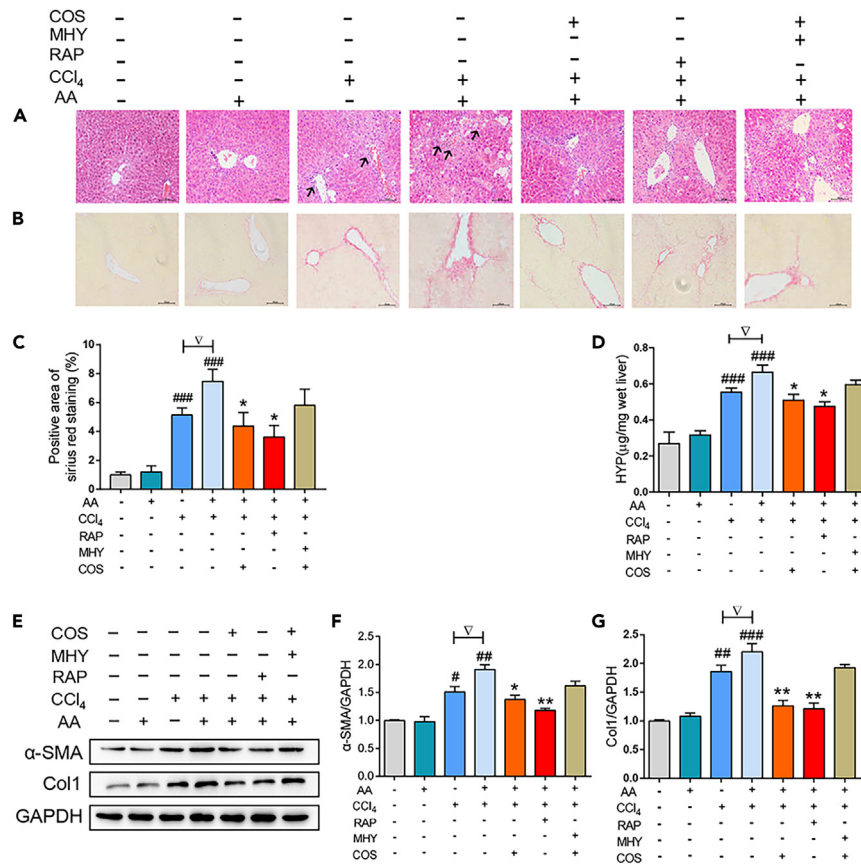
Figure 3. Improvement of hepatic fibrosis induced by combining Phe, Tyr, and CCl₄ in mice

(A and B) Hematoxylin-eosin and Sirius red staining of liver tissue (n = 6).

(C) Positive staining areas with Sirius red stain.

(D) The levels of HYP in liver tissue (n = 6).

(E) The protein levels of α-SMA and Col1 were analyzed via western blotting (n = 3).

(F and G) The grayscale analysis of α-SMA and Col1. All values are presented as means ± SEM. Significantly different (*p < 0.05, **p < 0.01, ***p < 0.001) compared with AA and CCl₄ treatment. Significantly different (#p < 0.05, ##p < 0.01, ###p < 0.001) compared with the CTL group. Significantly different (▽ p < 0.05) compared with CCl₄ treatment.

(Figures 5G–5I), in line with the influence of COS treatment on the mTORC1 pathway *in vivo* (Figure S6). It reported that transient inhibition of mTORC1 signaling by rapamycin inhibit cellular apoptosis, further against irradiation-induced liver damage,[28] suggesting that the activation of mTORC1 pathway might promote the hepatocyte apoptosis. In summary, this further emphasized that hepatocytes could be damaged by Phe and Tyr, which was responsible for the exacerbation of hepatic fibrosis, but the damage was reversed by COS treatment via the mTORC1 pathway.

Restriction of hyperactive fibroblasts

The activation of HSCs is the pivot of hepatic fibrosis admittedly, hence it is reasonable to explore the effects of Phe and Tyr on HSCs. Similarly, LX-2 cells were activated by Phe and Tyr at low concentrations (Figure S9). Furthermore, COS inhibited Phe- and Tyr-induced activation of LX-2 cells (Figures 6A–6C and S10). Given that the mTORC1 pathway is located at the intersection of amino acid homeostasis and the pathological process of hepatic fibrosis, the mTORC1 pathway was analyzed and was observed to be activated by Phe and Tyr (Figures 6A, 6D, and 6E). However, the activation effect of Phe and Tyr was prominently inhibited by RAP, suggesting that Phe and Tyr could induce LX-2 cell activation depending on the hyperactivation of the mTORC1 pathway (Figures 6F and 6G). Further, the fluctuation in the trend of α-SMA and Col1 levels also illustrated this mechanism (Figures 6H–6J). Additionally, the use of MHY also verified the mechanism of COS inhibition of the Phe- and Tyr-induced activation of LX-2 cells. MHY significantly activated LX-2 cells by upregulating the mTORC1 pathway, manifesting in the enhancement of α-SMA and Col1 levels, while the cascadic reactions of MHY were reversed by COS treatment (Figures 6K–6O). Taken together, these data showed that LX-2 cells could be induced into an activated state by Phe and Tyr through the mTORC1 pathway, but this was alleviated by COS treatment. The results were consistent with the aforementioned *in vivo* results.
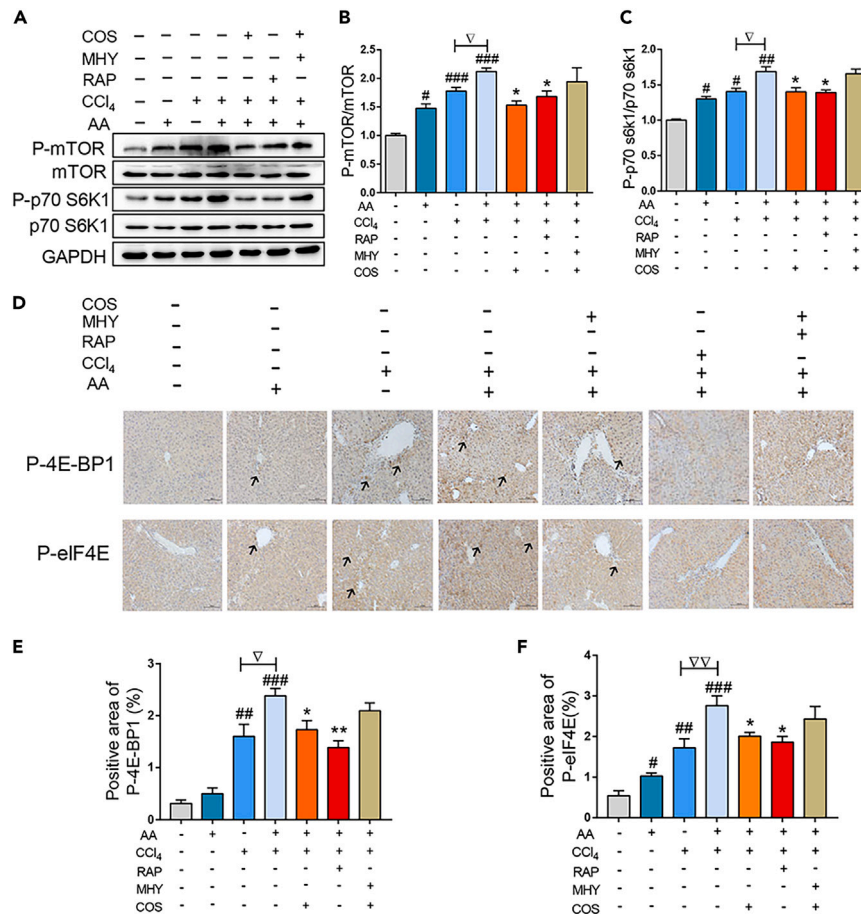
Figure 4. Amelioration of hepatic fibrosis induced by combining Phe, Tyr, and CCl₄ in mice by inhibiting the mTORC1 pathway

(A) The protein levels of P-mTOR, mTOR, P-p70 S6K1, and p70 S6K1 were explored by western blotting (n = 3).

(B and C) The grayscale analysis of P-mTOR and P-p70 S6K1.

(D) Immunohistochemical analysis of P-eIF4e and P-4EBP1 protein expression in liver (n = 6).

(E and F) Positive staining areas of P-eIF4e and P-4EBP1. All values are presented as means ± SEM. Significantly different (*$p < 0.05$, **$p < 0.01$, ***$p < 0.001$) compared with AA and CCl₄ treatment. Significantly different (#$p < 0.05$, ##$p < 0.01$, ###$p < 0.001$) compared with the CTL group. Significantly different ($\nabla p < 0.05$, $\nabla\nabla p < 0.01$) compared with CCl₄ treatment.

COS regulated the disruptive gut microecology caused by Phe and Tyr

Previous reports showed that gut microbes and their metabolites contribute jointly to the regulation of metabolism and organism functions in the host.[29–31] Many of these cascadic reactions depend on the mTORC1 pathway, which affects the gut microbial community structure in a feedback manner. Therefore, the gut microbiota and mTORC1 pathway could act in a synergetic manner.[32] Gut microbiota as a pivotal hub plays an increasingly crucial role in hepatic fibrosis progression. It can also accelerate metabolite production via fermentation to promote nutrient metabolism and synthesis.[33,34] Hence, gut microbiota is regarded as a prospective regulator of amino acid homeostasis. The finding showed that a total of 1,589,402 raw reads, with an average of 79,470 ± 6,392 reads per sample, were obtained. Partial least squares-discriminant analysis was performed to exhibit a holistic perception of the microbiota. The results obtained in the CTL, CCl₄, AA + CCl₄, and COS groups were separated into four clusters. The apparent clustering of microbiota composition in the CCl₄ group was distinct from that in the AA + CCl₄ group, suggesting a different biological community, and the gut microbiota of the AA + CCl₄ group exhibited a slight structural shift with COS treatment (Figures 7A and S11). Gut microbiota composition at the genus level was profoundly affected by the treatments, including *Dubosiella*, *Burkholderia-Caballeronia-Paraburkholderia*, *Enterococcus*, *Prevotella*, *Clostridia_vadinBB60_group*, and *Alistipes* (Figure 7B). Crucially, the *Clostridiales_vadinBB60_group* is closely related to the levels of urinary choline and phosphorylcholine, which are emerging as metabolic hallmarks of liver disease.[35] The abundances of *Alistipes* and *Prevotella* were highly correlated with amino acid metabolism and were also positively associated with inflammation- and oxidative stress-induced liver injury.[36–38] Furthermore, linear discriminant analysis (LDA) analysis suggested that at the genus level, gut microbiota structure was profoundly altered, exhibiting different intestinal microbial communities in various treatment groups (Figure 7C). These results suggested that stimulation with Tyr and Phe profoundly influenced the gut microbiota structure of mice with hepatic fibrosis, which was simultaneously affected by COS treatment.
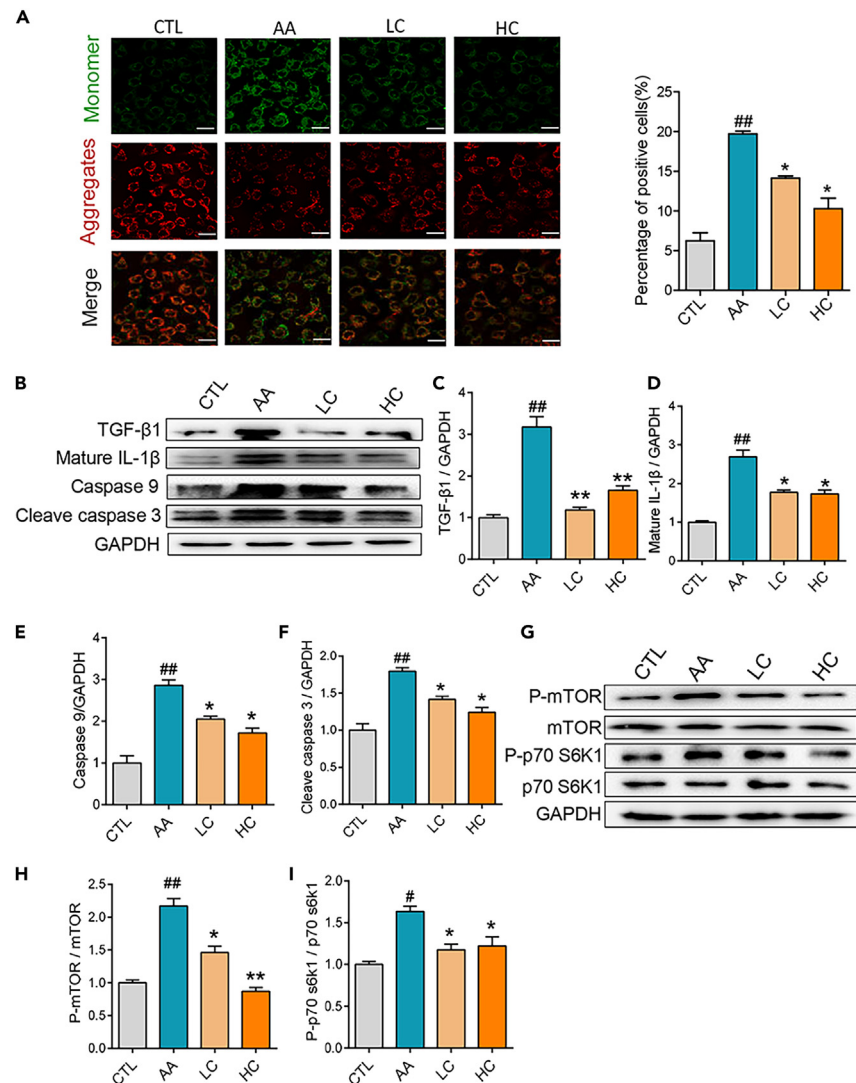
Figure 5. Reduction of Phe- and Tyr-induced damage in L-02 cells

(A–I) The mitochondrial membrane potential of L-02 cells was detected using a JC-1 probe (A). The protein levels of TGF-β1, mature IL-1β, caspase 9, and cleaved caspase 3 were analyzed by western blotting (B). The grayscale of TGF-β1 (C), mature IL-1β (D), caspase 9 (E), and cleaved caspase 3 (F). The pivotal protein levels in the mTORC1 pathway were analyzed by western blotting (G). The grayscale of P-mTOR (H) and P-p70 S6K1 (I). All values are presented as means ± SEM (n = 3). Significantly different (*$p < 0.05$, **$p < 0.01$) versus the AA group. Significantly different (#$p < 0.05$, ##$p < 0.01$) versus the CTL group.

To specifically identify the characteristic bacteria, 64 ASVs showed remarkable alterations in the CTL group compared with the AA + CCl_4 group, with 26 ASVs increased and 38 ASVs decreased (Figures 8A and 8B). Based on these 64 ASVs, the bacterial communities in the CCl_4 and COS groups were compared with those in the AA + CCl_4 group. In the AA + CCl_4 group, the relative abundances of the *Rikenella-ceae_RC9_gut_group*, *Oscillibacter*, *Colidextribacter*, Oscillospiraceae family (ASV116, ASV153, ASV168, ASV142), *Incertae_sedis*, *Eubacterium_siraeum_group*, UBA1819, *Eubacterium_coprostanoligenes_group*, *Blautia*, *Acetobacter*, Lachnospiraceae family (ASV220, ASV245, ASV168, ASV142, ASV261, ASV155, ASV52), *Eubacterium_xylanophilum_group*, and *Staphylococcus* were increased, while those of Muribaculaceae, Ruminococcaceae family (ASV86), *Ruminococcus*, GCA-900066575, and *Enterorhabdus* were decreased compared with those in the CCl_4 group. Among these, the relative abundances of *Oscillibacter*, ASV116 of Oscillospiraceae, *Incertae_sedis*, *Eubacterium_siraeum_group*, UBA1819, *Eubacterium_coprostanoligenes_group*, *Blautia*, *Acetobacter*, and Lachnospiraceae family (ASV220, ASV245, ASV155, ASV52) were reversed by COS treatment (Figure 8B). Distinct functions of altered ASVs were concurrently identified by PICRUSt2 analysis; 41 pathways were altered between the AA + CCl_4 and COS groups, among which the pathway of amino acid metabolism was the most altered (Figure S12A). Further analysis showed that 14 pathways of amino acid metabolism were affected, especially Phe metabolism, Tyr metabolism, and Phe, Tyr, and Trp biosynthesis (Figure S12B). Additionally, among the 64 ASVs, the relative abundances of 10 ASVs exhibited statistical differences between the AA + CCl_4 and COS groups. Noticeably, these 10 ASVs mainly belonged to the families
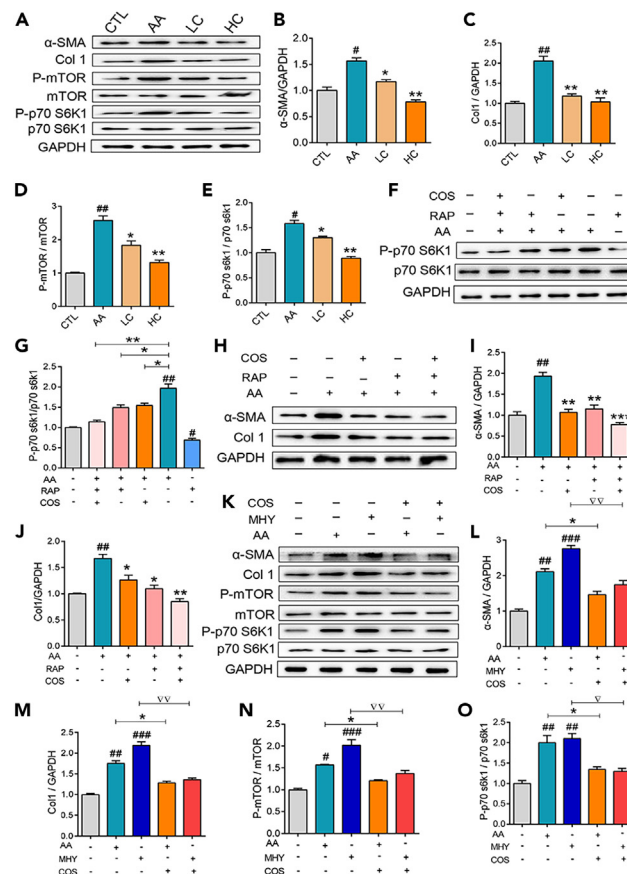
Figure 6. Amelioration of Phe- and Tyr-induced activation of LX-2 cells by downregulating the mTORC1 pathway

(A–O) The protein levels of α-SMA, Col1, P-mTOR, mTOR, P-p70 S6K1, and p70 S6K1 were explored by western blotting (A) The grayscale of α-SMA (B), Col1 (C), P-mTOR (D), and P-p70 S6K1 (E) After applying RAP (F–J) and MHY (K–O), the protein levels of α-SMA, Col1, P-mTOR, mTOR, P-p70 S6K1, and p70 S6K1 were also determined and analyzed. All values are presented as means ± SEM (n = 3). Significantly different (*p < 0.05, **p < 0.01, ***p < 0.001) versus the AA group. Significantly different (#p < 0.05, ##p < 0.01, ###p < 0.01) versus the CTL group. Significantly different (∇p < 0.05, ∇∇p < 0.01) versus the MHY group.

Oscillospiraceae, Ruminococcaceae, and Lachnospiraceae (Figure S13A). A heatmap of the relationship among the altered gut microbiota, key indicators of the mTOR pathway, and pathological parameters related to hepatic fibrosis was generated, showing that all the 10 ASVs could improve liver function and inhibit mTOR activation, with ASV171, ASV79, ASV143, and ASV95 acting as key drivers (Figure S13B). In conclusion, dysbiosis of gut microbiota in hepatic fibrosis was aggravated by Tyr and Phe, with the families Oscillospiraceae, Ruminococcaceae, and Lachnospiraceae possibly mainly contributing to the protective effect of COS on Tyr- and Phe-mediated liver injury.

DISCUSSION

Hepatic fibrosis has been recognized as a wound-healing response by the liver. It is also reversible and dynamic according to clinical trials and theoretical analysis.[39] Recently, it has been investigated that hepatic fibrosis is associated with metabolic abnormalities, which initiate a biological cascadic reaction to modulate gene expression and changes in cellular function. COS, which have a hepatoprotective effect, also possess the ability to ameliorate hepatic fibrosis,[21] however, the precise mechanism is unclear, especially regarding to the regulation of metabolites in hepatic fibrosis.

CCl₄ is one of the standardized and also most used hepatotoxins for hepatic fibrosis modeling establishment. It is metabolically activated in hepatocytes by P450 cytochromes, mainly CYP2El, leading to the formation of trichloromethyl radicals, which would trigger hepatocyte death via lipid peroxidation and thus induce robust and rapid fibrosis.[40] Herein, CCl₄ was applied to induce hepatic fibrosis model, and metabolite mapping and quantitative analysis revealed that COS alleviated hepatic fibrosis by regulating amino acid metabolism homeostasis, especially Phe and Tyr. The levels of Phe and Tyr in the serum were increased by CCl₄ challenge, which were downregulated by COS treatment, but the level of Trp remained unchanged. Shikimic acid and chorismite, intermediates in the pathway of AAAs, act upstream of the crossroads of Phe and Trp. Shikimic and chorismite levels were increased in the CCl₄ group, which were reduced by COS treatment (results not shown). Hence, this deductively indicated that the increase of the levels of Phe and Tyr in mice with hepatic fibrosis may be caused by their
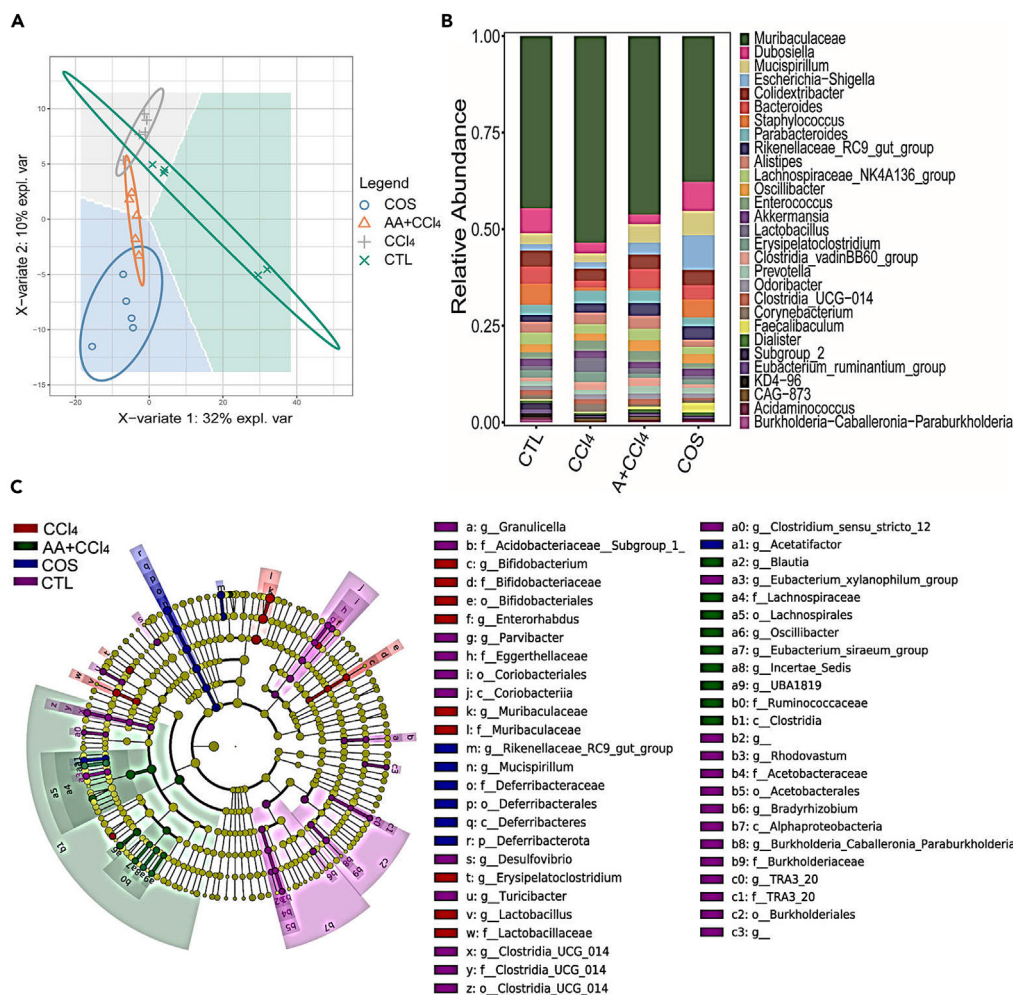
Figure 7. Regulation of gut microbiota composition
(A–C) Partial least squares-discriminant analysis (PLS-DA) of 16S rRNA genes (A). Composition of gut microbiota at the genus level (B). Cladogram representing the taxonomic hierarchical structure of the identified phylotype biomarkers generated by applying linear discriminant analysis effect size (LEfSe). Phylotypes statistically overrepresented in the different groups (C).

accumulation. Additionally, as Trp metabolism involves non-unique inducible enzymes, changes therein may be unpredictable in mice with hepatic fibrosis.[41] Most Phe is oxidized to Tyr, which is metabolized by rate-limiting hepatic enzymes, including TAT and TYR, and then further used to synthesize substances involved in lipid and carbohydrate metabolism.[41,42] COS indeed promoted the metabolism of Phe and Tyr, which might be attributed to the increase in the expression level of TAT, TYR, and PAH in this study. Previous studies showed that COS improved liver injury through antioxidant effect, regulating the polarization of M1 and M2 macrophages, etc.,[21,43] while the effects of COS in anti-hepatic fibrosis might be related to the decrease of Phe and Tyr levels in this study. It consistently confirmed that COS could regulate amino acid metabolism, especially by elevating gene expression levels and key enzyme activities, which further enhanced Phe metabolism.[44–46] Therefore, COS treatment-mediated improved hepatic fibrosis is primarily attributed to the reduction of Phe and Tyr levels.

Mounting evidence suggests that high concentrations of Phe and Tyr can exacerbate oxidative stress and inflammation.[47,48] Increased concentrations of Phe and Tyr represent potential biomarkers for a number of cancers.[49] Critically, these cascadic effects may be specific to these two amino acids, which could participate in the regulation of cellular signals. This study further found that Phe and Tyr treatment in mice with hepatic fibrosis deteriorated pathological symptoms. Interestingly, COS treatment alleviated Phe- and Tyr-induced liver dysfunction by inhibiting the mTORC1 pathway and repaired the gut microecology. The mTORC1 pathway responds sensitively to amino acids, as a foreground biomarker and target in hepatic fibrosis. Activation of the mTORC1 pathway represents a pivotal signal hub during hepatic fibrogenesis and contributes to the *trans*-differentiation of HSCs.[17] Therefore, the mTORC1 pathway is located at the crossroads. COS coincidently restored the hyperactivation of the mTORC1 pathway, contributing to Phe- and Tyr-induced liver injury. A recent study coincidently showed that COS resisted oxidative stress by accelerating amino acid transport by upregulating the mTOR pathway.[50] It was also reported
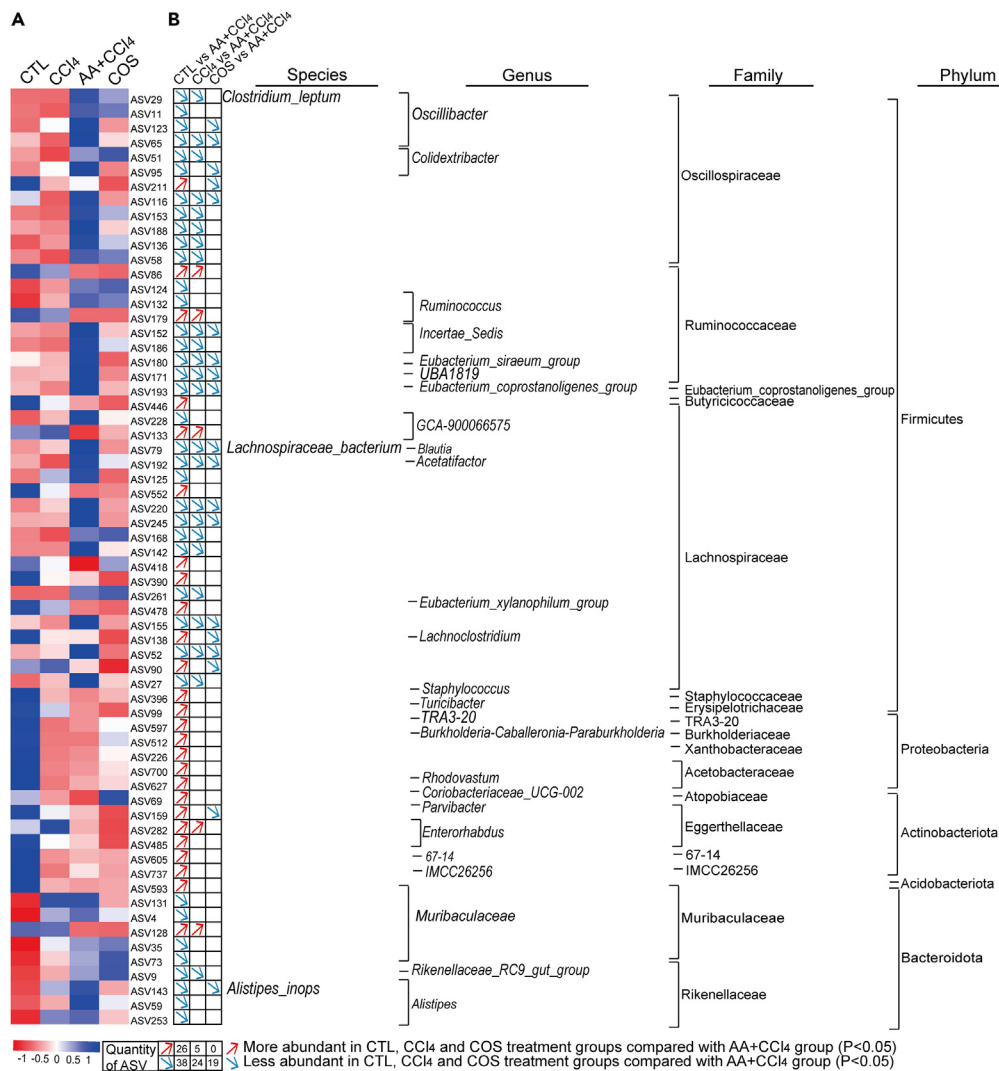
Figure 8. Pivotal ASVs modulated by Phe, Tyr, and COS

(A and B) Heatmap showing the abundance of 64 ASVs found to be significantly different between the CTL and AA + CCl4 groups (A). Represented bacterial taxonomic information from panel A. Significantly different (red and blue arrows, p < 0.05) compared with the AA + CCl4 group (B).

that COS could sensitively block the hyperactivation of the mTORC1 pathway to fight against endoplasmic reticulum stress-induced apoptosis.[51]

Similarly, gut microbiota acts as a pivotal hub in hepatic fibrosis progression and amino acid synthesis. In this study, dysbiosis of gut microbiota in hepatic fibrosis aggravated by Tyr and Phe was reversed by COS treatment, and this was mainly attributed to the reduced relative abundances of *Oscillibacter*, *Incertae_sedis*, *Eubacterium_siraeum_group*, UBA1819, *Eubacterium_coprostanoligenes_group*, *Blautia*, and *Acetobacter*. Previous studies have consistently indicated that COS acts as a prominently moderator in AAAs metabolism through regulating gut microbes.[45] Some gut microbiota is substantially associated with alterations in plasma metabolites, particularly in those of amino acids, including *Oscillibacter*, *Eubacteriumcoprostanoligenes_group*, and *Blautia*.[52–56] Moreover, an increase in the abundance of *Oscillibacter* is related to the activation of the mTORC1 pathway.[57,58] Alterations in gut microbiota accompanied by metabolite disorders could indeed enhance glucose production and further cause the overactivation of mTORC1 pathway in hepatocytes.[57,58] Conclusively, the COS treatment-mediated improved Tyr- and Phe-mediated liver injury was attributed to blockade of mTORC1 pathway activation and remission of the dysbiosis of gut microbiota.

Conclusion

Conclusively, hepatic fibrosis is accompanied by amino acid metabolism disorder, especially increases in Phe and Tyr levels. Phe and Tyr exacerbated the severity of hepatic fibrosis and the dysbiosis of gut microbiota in hepatic fibrosis mice, suggesting that Phe and
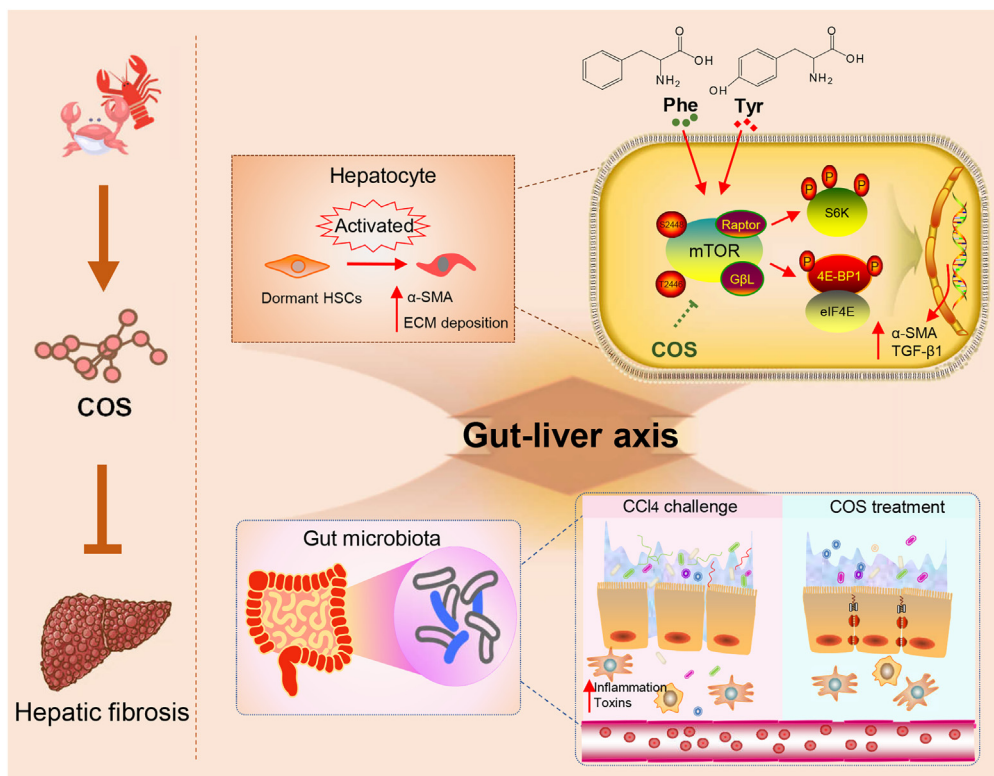
Figure 9. Schematic illustration of the potential mechanisms underlying the attenuation of hepatic fibrosis by COS.

Tyr acted to regulate cellular signal transduction in hepatic cells and profoundly influenced gut microbiota structure in hepatic fibrosis, providing a new insight on the role of Phe and Tyr in hepatic fibrosis. Additionally, COS treatment prominently alleviated CCl_4-induced hepatic fibrosis by reducing serum levels of Phe and Tyr as well as relieved Phe- and Tyr-induced liver dysfunction by downregulating the mTORC1 pathway (Figure 9). Our study clarifies the unclear role of COS in hepatopathy, paving the way for the treatment of hepatic fibrosis with COS.

Limitations of the study

This study aimed to provide insight into the effectiveness and molecular mechanism of COS in the intervention of hepatic fibrosis from the perspective of metabolites. The availability of different COS monomers and the molecular targets (such as the target sites of mTORC1) for their anti-fibrosis effect remain to be elucidated. Experiments probing the influence of the intestinal microecology should be conducted to further provide important mechanistic insights.

STAR★METHODS

Detailed methods are provided in the online version of this paper and include the following:

- KEY RESOURCES TABLE
- RESOURCE AVAILABILITY
  - Lead contact
  - Material availability
  - Data and code availability
- EXPERIMENTAL MODEL AND SUBJECT DETAILS
  - Mouse model
  - Establishment of hepatic fibrosis model
  - Influence evaluation and scheme exploration of Phe and Tyr
  - Cell culture and treatment
  - Induction of hepatocyte damage by H_2O_2
  - Treatment with Phe and Tyr

- METHOD DETAILS
  - Mitochondrial membrane potential analysis
  - Determination of aromatic amino acid levels by HPLC
  - Serum metabolite profiling
  - 16S rRNA gene pyrosequencing and analysis
  - Histopathological and immunohistochemical analysis
  - Western blotting analysis
  - Quantitative real-time PCR (qRT-PCR) assay
- QUANTIFICATION AND STATISTICAL ANALYSIS

SUPPLEMENTAL INFORMATION

Supplemental information can be found online at https://doi.org/10.1016/j.isci.2023.107754.

ACKNOWLEDGMENTS

AUTHOR CONTRIBUTIONS

P.L.: Methodology, Roles/Writing-original draft; H.L.: Conceptualization, Data curation, Writing-review & editing, Funding acquisition; H.X.: Investigation, Visualization; J.G.: Supervision, Data curation; M.J.: Visualization, Data curation; Z.X.: Visualization, Funding acquisition; J.S.: Conceptualization, Funding acquisition, Project administration.

DECLARATION OF INTERESTS

The authors declare no competing interests.

INCLUSION AND DIVERSITY

We support inclusive, diverse, and equitable conduct of research.

REFERENCES

1. Roehlen, N., Crouchet, E., and Baumert, T.F. (2020). Liver Fibrosis: Mechanistic Concepts and Therapeutic Perspectives. Cells 9. https://doi.org/10.3390/cells9040875.

2. Patel, P.J., Connoley, D., Rhodes, F., Srivastava, A., and Rosenberg, W. (2020). A review of the clinical utility of the Enhanced Liver Fibrosis test in multiple aetiologies of chronic liver disease. Ann. Clin. Biochem. 57, 36–43. https://doi.org/10.1177/0004563219879962.

3. Shi, Z., Zhang, K., Chen, T., Zhang, Y., Du, X., Zhao, Y., Shao, S., Zheng, L., Han, T., and Hong, W. (2020). Transcriptional factor ATF3 promotes liver fibrosis via activating hepatic stellate cells. Cell Death Dis. 11, 1066. https://doi.org/10.1038/s41419-020-03271-6.

4. Kisseleva, T., and Brenner, D. (2021). Molecular and cellular mechanisms of liver fibrosis and its regression. Nat. Rev. Gastroenterol. Hepatol. 18, 151–166. https://doi.org/10.1038/s41575-020-00372-7.

5. Lee, Y.A., Wallace, M.C., and Friedman, S.L. (2015). Pathobiology of liver fibrosis: a translational success story. Gut 64, 830–841. https://doi.org/10.1136/gutjnl-2014-306842.

6. Bizeau, M.E., and Pagliassotti, M.J. (2005). Hepatic adaptations to sucrose and fructose.

Metabolism 54, 1189–1201. https://doi.org/10.1016/j.metabol.2005.04.004.

7. Wanninger, J., Neumeier, M., Hellerbrand, C., Schacherer, D., Bauer, S., Weiss, T.S., Huber, H., Schäffler, A., Aslanidis, C., Schölmerich, J., and Buechler, C. (2011). Lipid accumulation impairs adiponectin-mediated induction of activin A by increasing TGFbeta in primary human hepatocytes. Biochim. Biophys. Acta 1811, 626–633. https://doi.org/10.1016/j.bbalip.2010.11.001.

8. Zhang, Y., Zhao, M., Liu, Y., Liu, T., Zhao, C., and Wang, M. (2021). Investigation of the therapeutic effect of Yinchen Wuling Powder on CCl4-induced hepatic fibrosis in rats by (1) H NMR and MS-based metabolomics analysis. J. Pharm. Biomed. Anal. 200, 114073. https://doi.org/10.1016/j.jpba.2021.114073.

9. Nault, R., Fader, K.A., Ammendolia, D.A., Dornbos, P., Potter, D., Sharratt, B., Kumagai, K., Harkema, J.R., Lunt, S.Y., Matthews, J., and Zacharewski, T. (2016). Dose-Dependent Metabolic Reprogramming and Differential Gene Expression in TCDD-Elicited Hepatic Fibrosis. Toxicol. Sci. 154, 253–266. https://doi.org/10.1093/toxsci/kfw163.

10. Jiang, H., Song, J.M., Gao, P.F., Qin, X.J., Xu, S.Z., and Zhang, J.F. (2017). Metabolic characterization of the early stage of hepatic fibrosis in rat using GC-TOF/MS and multivariate data analyses. Biomed. Chromatogr. 31, e3899. https://doi.org/10.1002/bmc.3899.

11. Chang, M.L., and Yang, S.S. (2019). Metabolic Signature of Hepatic Fibrosis: From Individual Pathways to Systems Biology. Cells 8. https://doi.org/10.3390/cells8111423.

12. Tajiri, K., and Shimizu, Y. (2018). Branched-chain amino acids in liver diseases. Transl. Gastroenterol. Hepatol. 3, 47. https://doi.org/10.21037/tgh.2018.07.06.

13. Shcherbakova, E.S., Sall, T.S., Sitkin, S.I., Vakhitov, T.Y., and Demyanova, E.V. (2020). The role of bacterial metabolites derived from aromatic amino acids in non-alcoholic fatty liver disease. Al'm. klin. med. 48, 375–386. https://doi.org/10.18786/2072-0505-2020-48-066.

14. Heianza, Y., Sun, D., Li, X., DiDonato, J.A., Bray, G.A., Sacks, F.M., and Qi, L. (2019). Gut microbiota metabolites, amino acid metabolites and improvements in insulin sensitivity and glucose metabolism: the

POUNDS Lost trial. Gut 68, 263–270. https://doi.org/10.1136/gutjnl-2018-316155.

15. Battaglioni, S., Benjamin, D., Wälchli, M., Maier, T., and Hall, M.N. (2022). mTOR substrate phosphorylation in growth control. Cell 185, 1814–1836. https://doi.org/10.1016/j.cell.2022.04.013.

16. Sancak, Y., Bar-Peled, L., Zoncu, R., Markhard, A.L., Nada, S., and Sabatini, D.M. (2010). Ragulator-Rag complex targets mTORC1 to the lysosomal surface and is necessary for its activation by amino acids. Cell 141, 290–303. https://doi.org/10.1016/j.cell.2010.02.024.

17. Luo, J.T., Zhu, S.C., Huang, Y.L., Ye, J.P., and Shen, S. (2021). [Exploring the effects of artesunate and fuzheng huayu decoction on mitochondria in the treatment of schistosomiasis liver fibrosis]. Zhonghua Gan Zang Bing Za Zhi 29, 148–154. https://doi.org/10.3760/cma.j.cn501113-20201024-00577.

18. Yeh, M.Y., Shang, H.S., Lu, H.F., Chou, J., Yeh, C., Chang, J.B., Hung, H.F., Kuo, W.L., Wu, L.Y., and Chung, J.G. (2015). Chitosan oligosaccharides in combination with Agaricus blazei Murill extract reduces hepatoma formation in mice with severe combined immunodeficiency. Mol. Med. Rep. 12, 133–140. https://doi.org/10.3892/mmr.2015.3454.

19. Bai, Y., Zheng, J., Yuan, X., Jiao, S., Feng, C., Du, Y., Liu, H., and Zheng, L. (2018). Chitosan Oligosaccharides Improve Glucolipid Metabolism Disorder in Liver by Suppression of Obesity-Related Inflammation and Restoration of Peroxisome Proliferator-Activated Receptor Gamma (PPARgamma). Mar. Drugs 16, 455. https://doi.org/10.3390/md16110455.

20. Luo, Z., Dong, X., Ke, Q., Duan, Q., and Shen, L. (2014). Chitooligosaccharides inhibit ethanol-induced oxidative stress via activation of Nrf2 and reduction of MAPK phosphorylation. Oncol. Rep. 32, 2215–2222. https://doi.org/10.3892/or.2014.3463.

21. Liu, P., Li, H., Gong, J., Geng, Y., Jiang, M., Xu, H., Xu, Z., and Shi, J. (2022). Chitooligosaccharides alleviate hepatic fibrosis by regulating the polarization of M1 and M2 macrophages. Food Funct. 13, 753–768. https://doi.org/10.1039/d1fo03768d.

22. Liu, P., Li, H., Li, R., Geng, Y., Gong, J., Xu, H., Xu, Z., and Shi, J. (2022). Nanoencapsulation of chitooligosaccharides enhances its oral bioavailability and anti-liver fibrotic effects. Food Res. Int. 157, 111471. https://doi.org/10.1016/j.foodres.2022.111471.

23. Haufe, S., Witt, H., Engeli, S., Kaminski, J., Utz, W., Fuhrmann, J.C., Rein, D., Schulz-Menger, J., Luft, F.C., Boschmann, M., and Jordan, J. (2016). Branched-chain and aromatic amino acids, insulin resistance and liver specific ectopic fat storage in overweight to obese subjects. Nutr. Metabol. Cardiovasc. Dis. 26, 637–642. https://doi.org/10.1016/j.numecd.2016.03.013.

24. Parés, A., Deulofeu, R., Cisneros, L., Escorsell, A., Salmerón, J.M., Caballería, J., and Mas, A. (2009). Albumin dialysis improves hepatic encephalopathy and decreases circulating phenolic aromatic amino acids in patients with alcoholic hepatitis and severe liver failure. Crit. Care 13, R8. https://doi.org/10.1186/cc7697.

25. Xiao, Y., Wang, Y., Liu, Y., Wang, W., Tian, X., Chen, S., Lu, Y., Du, J., and Cai, W. (2021). A nonbile acid farnesoid X receptor agonist tropifexor potently inhibits cholestatic liver injury and fibrosis by modulating the gut-liver axis. Liver Int. 41, 2117–2131. https://doi.org/10.1111/liv.14906.

26. Dejong, C.H.C., van de Poll, M.C.G., Soeters, P.B., Jalan, R., and Olde Damink, S.W.M. (2007). Aromatic amino acid metabolism during liver failure. J. Nutr. 137, 1579s–1585s.

27. Wang, W., Yan, J., Wang, H., Shi, M., Zhang, M., Yang, W., Peng, C., and Li, H. (2014). Rapamycin ameliorates inflammation and fibrosis in the early phase of cirrhotic portal hypertension in rats through inhibition of mTORC1 but not mTORC2. PLoS One 9, e83908. https://doi.org/10.1371/journal.pone.0083908.

28. Yang, W., Shao, L., Zhu, S., Li, H., Zhang, X., Ding, C., Wu, X., Xu, R., Yue, M., Tang, J., et al. (2019). Transient Inhibition of mTORC1 Signaling Ameliorates Irradiation-Induced Liver Damage. Front. Physiol. 10, 228. https://doi.org/10.3389/fphys.2019.00228.

29. Parker, A., Fonseca, S., and Carding, S.R. (2020). Gut microbes and metabolites as modulators of blood-brain barrier integrity and brain health. Gut Microb. 11, 135–157. https://doi.org/10.1080/19490976.2019.1638722.

30. Wang, F., Song, M., Lu, X., Zhu, X., and Deng, J. (2022). Gut microbes in gastrointestinal cancers. Semin. Cancer Biol. 86, 967–975. https://doi.org/10.1016/j.semcancer.2021.03.037.

31. Rastogi, S., Mohanty, S., Sharma, S., and Tripathi, P. (2022). Possible role of gut microbes and host's immune response in gut-lung homeostasis. Front. Immunol. 13, 954339. https://doi.org/10.3389/fimmu.2022.954339.

32. Noureldein, M.H., and Eid, A.A. (2018). Gut microbiota and mTOR signaling: Insight on a new pathophysiological interaction. Microb. Pathog. 118, 98–104. https://doi.org/10.1016/j.micpath.2018.03.021.

33. Chen, H., Li, C., Liu, T., Chen, S., and Xiao, H. (2020). A Metagenomic Study of Intestinal Microbial Diversity in Relation to Feeding Habits of Surface and Cave-Dwelling Sinocyclocheilus Species. Microb. Ecol. 79, 299–311. https://doi.org/10.1007/s00248-019-01409-4.

34. Zheng, H., You, Y., Hua, M., Wu, P., Liu, Y., Chen, Z., Zhang, L., Wei, H., Li, Y., Luo, M., et al. (2018). Chlorophyllin Modulates Gut Microbiota and Inhibits Intestinal Inflammation to Ameliorate Hepatic Fibrosis in Mice. Front. Physiol. 9, 1671. https://doi.org/10.3389/fphys.2018.01671.

35. Nicholson, J.K., Holmes, E., Kinross, J., Burcelin, R., Gibson, G., Jia, W., and Pettersson, S. (2012). Host-gut microbiota metabolic interactions. Science 336, 1262–1267. https://doi.org/10.1126/science.1223813.

36. He, Z., Wu, J., Xiao, B., Xiao, S., Li, H., and Wu, K. (2019). The Initial Oral Microbiota of Neonates Among Subjects With Gestational Diabetes Mellitus. Front. Pediatr. 7, 513. https://doi.org/10.3389/fped.2019.00513.

37. Xue, M.Y., Sun, H.Z., Wu, X.H., Liu, J.X., and Guan, L.L. (2020). Multi-omics reveals that the rumen microbiome and its metabolome together with the host metabolome contribute to individualized dairy cow performance. Microbiome 8, 64. https://doi.org/10.1186/s40168-020-00819-8.

38. Moschen, A.R., Gerner, R.R., Wang, J., Klepsch, V., Adolph, T.E., Reider, S.J., Hackl, H., Pfister, A., Schilling, J., Moser, P.L., et al. (2016). Lipocalin 2 Protects from Inflammation and Tumorigenesis Associated with Gut Microbiota Alterations. Cell Host Microbe 19, 455–469. https://doi.org/10.1016/j.chom.2016.03.007.

39. Schuppan, D., and Kim, Y.O. (2013). Evolving therapies for liver fibrosis. J. Clin. Invest. 123, 1887–1901. https://doi.org/10.1172/JCI66028.

40. Ravichandra, A., and Schwabe, R.F. (2021). Mouse Models of Liver Fibrosis. Methods Mol. Biol. 2299, 339–356. https://doi.org/10.1007/978-1-0716-1382-5_23.

41. Krzyściak, W. (2011). Activity of selected aromatic amino acids in biological systems. Acta Biochim. Pol. 58, 461–466.

42. Loza-Valdes, A., Mayer, A.E., Kassouf, T., Trujillo-Viera, J., Schmitz, W., Dziaczkowski, F., Leitges, M., Schlosser, A., and Sumara, G. (2021). A phosphoproteomic approach reveals that PKD3 controls PKA-mediated glucose and tyrosine metabolism. Life Sci. Alliance 4, e202000863. https://doi.org/10.26508/lsa.202000863.

43. Wang, Y., Xiong, Y., Zhang, A., Zhao, N., Zhang, J., Zhao, D., Yu, Z., Xu, N., Yin, Y., Luan, X., and Xiong, Y. (2020). Oligosaccharide attenuates aging-related liver dysfunction by activating Nrf2 antioxidant signaling. Food Sci. Nutr. 8, 3872–3881. https://doi.org/10.1002/fsn3.1681.

44. Liu, W., Li, X., Zhao, Z., Pi, X., Meng, Y., Fei, D., Liu, D., and Wang, X. (2020). Effect of chitooligosaccharides on human gut microbiota and antiglycation. Carbohydr. Polym. 242, 116413. https://doi.org/10.1016/j.carbpol.2020.116413.

45. Ji, X., Zhu, L., Chang, K., Zhang, R., Chen, Y., Yin, H., Jin, J., and Zhao, L. (2022). Chitooligosaccharides: Digestion characterization and effect of the degree of polymerization on gut microorganisms to manage the metabolome functional diversity in vitro. Carbohydr. Polym. 275, 118716. https://doi.org/10.1016/j.carbpol.2021.118716.

46. Yu, L., Zong, Y., Han, Y., Zhang, X., Zhu, Y., Oyom, W., Gong, D., Prusky, D., and Bi, Y. (2022). Both chitosan and chitooligosaccharide treatments accelerate wound healing of pear fruit by activating phenylpropanoid metabolism. Int. J. Biol. Macromol. 205, 483–490. https://doi.org/10.1016/j.ijbiomac.2022.02.098.

47. Fuchs, J.E., Huber, R.G., von Grafenstein, S., Wallnoefer, H.G., Spitzer, G.M., Fuchs, D., and Liedl, K.R. (2012). Dynamic regulation of phenylalanine hydroxylase by simulated redox manipulation. PLoS One 7, e53005. https://doi.org/10.1371/journal.pone.0053005.

48. Moraes, T.B., Dalazen, G.R., Jacques, C.E., de Freitas, R.S., Rosa, A.P., and Dutra-Filho, C.S. (2014). Glutathione metabolism enzymes in brain and liver of hyperphenylalaninemic rats and the effect of lipoic acid treatment. Metab. Brain Dis. 29, 609–615. https://doi.org/10.1007/s11011-014-9491-x.

49. Wiggins, T., Kumar, S., Markar, S.R., Antonowicz, S., and Hanna, G.B. (2015). Tyrosine, phenylalanine, and tryptophan in gastroesophageal malignancy: a systematic review. Cancer Epidemiol. Biomarkers Prev. 24, 32–38. https://doi.org/10.1158/1055-9965.EPI-14-0980.

50. Xie, C., Wu, X., Long, C., Wang, Q., Fan, Z., Li, S., and Yin, Y. (2016). Chitosan oligosaccharide affects antioxidant defense capacity and placental amino acids transport

of sows. BMC Vet. Res. *12*, 243. https://doi.org/10.1186/s12917-016-0872-8.

51. Fang, T., Yao, Y., Tian, G., Chen, D., Wu, A., He, J., Zheng, P., Mao, X., Yu, J., Luo, Y., et al. (2021). Chitosan oligosaccharide attenuates endoplasmic reticulum stress-associated intestinal apoptosis via the Akt/mTOR pathway. Food Funct. *12*, 8647–8658. https://doi.org/10.1039/d1fo01234g.

52. Chen, L., Chen, D.Q., Liu, J.R., Zhang, J., Vaziri, N.D., Zhuang, S., Chen, H., Feng, Y.L., Guo, Y., and Zhao, Y.Y. (2019). Unilateral ureteral obstruction causes gut microbial dysbiosis and metabolome disorders contributing to tubulointerstitial fibrosis. Exp. Mol. Med. *51*, 1–18. https://doi.org/10.1038/s12276-019-0234-2.

53. Yu, M., Jia, H., Zhou, C., Yang, Y., Zhao, Y., Yang, M., and Zou, Z. (2017). Variations in gut microbiota and fecal metabolic phenotype associated with depression by 16S rRNA gene sequencing and LC/MS-based metabolomics. J. Pharm. Biomed. Anal. *138*, 231–239. https://doi.org/10.1016/j.jpba.2017.02.008.

54. Fang, S., Chen, X., Pan, J., Chen, Q., Zhou, L., Wang, C., Xiao, T., and Gan, Q.F. (2020). Dynamic distribution of gut microbiota in meat rabbits at different growth stages and relationship with average daily gain (ADG). BMC Microbiol. *20*, 116. https://doi.org/10.1186/s12866-020-01797-5.

55. Yang, J., Zheng, P., Li, Y., Wu, J., Tan, X., Zhou, J., Sun, Z., Chen, X., Zhang, G., Zhang, H., et al. (2020). Landscapes of bacterial and metabolic signatures and their interaction in major depressive disorders. Sci. Adv. *6*, eaba8555. https://doi.org/10.1126/sciadv.aba8555.

56. De Angelis, M., Piccolo, M., Vannini, L., Siragusa, S., De Giacomo, A., Serrazzanetti, D.I., Cristofori, F., Guerzoni, M.E., Gobbetti, M., and Francavilla, R. (2013). Fecal microbiota and metabolome of children with autism and pervasive developmental disorder not otherwise specified. PLoS One *8*, e76993. https://doi.org/10.1371/journal.pone.0076993.

57. Choi, B.S.Y., Daniel, N., Houde, V.P., Ouellette, A., Marcotte, B., Varin, T.V., Vors, C., Feutry, P., Ilkayeva, O., Ståhlman, M., et al. (2021). Feeding diversified protein sources exacerbates hepatic insulin resistance via increased gut microbial branched-chain fatty acids and mTORC1 signaling in obese mice. Nat. Commun. *12*, 3377. https://doi.org/10.1038/s41467-021-23782-w.

58. Jung, M.J., Lee, J., Shin, N.R., Kim, M.S., Hyun, D.W., Yun, J.H., Kim, P.S., Whon, T.W., and Bae, J.W. (2016). Chronic Repression of mTOR Complex 2 Induces Changes in the Gut Microbiota of Diet-induced Obese Mice. Sci. Rep. *6*, 30887. https://doi.org/10.1038/srep30887.

59. Kim, Y.O., Popov, Y., and Schuppan, D. (2017). Optimized Mouse Models for Liver Fibrosis. Methods Mol. Biol. *1559*, 279–296. https://doi.org/10.1007/978-1-4939-6786-5_19.

60. Zhang, J.W., Zhao, F., and Sun, Q. (2018). Metformin synergizes with rapamycin to inhibit the growth of pancreatic cancer in vitro and in vivo. Oncol. Lett. *15*, 1811–1816. https://doi.org/10.3892/ol.2017.7444.

61. Madrakhimov, S.B., Yang, J.Y., Kim, J.H., Han, J.W., and Park, T.K. (2021). mTOR-dependent dysregulation of autophagy contributes to the retinal ganglion cell loss in streptozotocin-induced diabetic retinopathy. Cell Commun. Signal. *19*, 29. https://doi.org/10.1186/s12964-020-00698-4.

62. Niu, H., Wang, J., Li, H., and He, P. (2011). Rapamycin potentiates cytotoxicity by docetaxel possibly through downregulation of Survivin in lung cancer cells. J. Exp. Clin. Cancer Res. *30*, 28. https://doi.org/10.1186/1756-9966-30-28.

63. Gao, L., Lv, G., Li, R., Liu, W.T., Zong, C., Ye, F., Li, X.Y., Yang, X., Jiang, J.H., Hou, X.J., et al. (2019). Glycochenodeoxycholate promotes hepatocellular carcinoma invasion and migration by AMPK/mTOR dependent autophagy activation. Cancer Lett. *454*, 215–223. https://doi.org/10.1016/j.canlet.2019.04.009.

STAR★METHODS

KEY RESOURCES TABLE

REAGENT or RESOURCE	SOURCE	IDENTIFIER
Antibodies		
Mature interleukin 1 beta (IL-1β)	Cell Signaling Technology	83186, RRID:AB_2800010
α-smooth muscle actin (α-SMA)	Cell Signaling Technology	19245, RRID:AB_2734735
Cleaved caspase 3	Cell Signaling Technology	9661, RRID:AB_2341188
Caspase 9	Cell Signaling Technology	9508, RRID:AB_2068620
mTOR	Cell Signaling Technology	2983, RRID:AB_2105622
phospho-mTOR	Cell Signaling Technology	5536, RRID:AB_10691552
p70 S6K1	Cell Signaling Technology	9202, RRID:AB_331676
phospho-p70 S6K1	Cell Signaling Technology	9204, RRID:AB_2265913
Glyceraldehyde-3-phosphate dehydrogenase (GAPDH)	Cell Signaling Technology	2118, RRID:AB_561053
Tumor necrosis factor alpha (TNF-α)	Abcam Technology	ab66579, RRID: AB_1310759
Type I collagen (Col1)	Abcam Technology	ab260043, AB_2922767
Phospho-eukaryotic translation initiation factor 4E (eIF4E)	Abcam Technology	ab76256, RRID:AB_1523534
Transforming growth factor β1 (TGF-β1)	Abcam Technology	ab31013, RRID:AB_778352
phospho- eIF4E-binding protein 1 (4E-BP1)	Thermo Fisher Scientific	PA5-38096, RRID:AB_2554699
Chemicals, peptides, and recombinant proteins		
COS	Yangzhou Rixing Bio-Tech Co	N/A
Phenylalanine (Phe)	Sigma-Aldrich	P1150000
Tyrosine (Tyr)	Sigma-Aldrich	T2900000
JC-1 probe	Beyotime Institute of Biotechnology	C2005
4,6-Di(4-morpholinyl)-N-(4-nitrophenyl)-1,3,5-triazin-2-amine (MHY1485)	MedChemExpress	HY-B0795
Rapamycin	MedChemExpress	HY-10219
Critical commercial assays		
5× All-In-One RT Master Mix kit	Applied Biological Materials	G592
SuperSignal™ West Pico PLUS	Thermo Fisher Scientific	34580
Deposited data		
Raw and analyzed data	This paper	Mendeley Data: https://doi.org/10.17632/y5bnz99t7b.1.
Experimental models: Cell lines		
hepatic cell line (L-02 cells)	ATCC	CBP60224
Hepatic stellate cells (LX-2 cells)	BeNa Culture Collection	BNCC337957
Experimental models: Organisms/strains		
Male C57BL/6J mice	Shanghai SLAC Laboratory Animal Co., Ltd	000664
Recombinant DNA		
Primers for quantitative real-time PCR, see Table 1	This paper	N/A
Software and algorithm		
ImageJ	https://ImageJ.nih.gov/	N/A

(Continued on next page)

Continued

REAGENT or RESOURCE	SOURCE	IDENTIFIER
GraphPad Prism version 8.0.1	Graphpad	N/A
SPSS version 21.0	SPSS	N/A
R packages	R Foundation for Statistical Computing	N/A

RESOURCE AVAILABILITY

Lead contact

Further information and requests for reagents and resources should be directed to and will be fulfilled by the lead contact, Heng Li (liheng@jiangnan.edu.cn).

Material availability

This study did not generate new unique reagents.

Data and code availability

- Data: the original data have been deposited at Mendeley Data and is publicly available as of the date of publication. The DOI is listed in the key resources table.
- Code: the paper did not generate original code.
- All other items: any additional information in this paper is available from the lead contact upon reasonable request.

EXPERIMENTAL MODEL AND SUBJECT DETAILS

Mouse model

Male C57BL/6J mice with (20 g $\pm$ 3 g) and 6–8 weeks old were handled according to the Guide for the Care and Use of Laboratory Animals published by the National Institutes of Health, and the experimental protocols were allowed by the related ethical regulations of Jiangnan University, with the permission number JN.No20220315c0720505[032]. Mice were employed with good reliability and repeatability for modeling, which were purchased from Shanghai SLAC Laboratory Animal Co., Ltd. (Shanghai, China).[21,22]

Establishment of hepatic fibrosis model

Mouse model has been admittedly regarded as indispensable in clarifying the mechanisms of hepatic fibrosis and can mimic critical symptoms of hepatic fibrosis, such as transcriptomic changes and cellular interaction.[40] CCl_4 is typically used to generate hepatic fibrosis model because it can induce robust fibrosis in a reasonable time frame. CCl_4 can be metabolized by hepatocytes, and its toxic metabolites contribute to cell damage, inflammation, and subsequently fibrogenic reaction. Moreover, cell necrosis, the main feature caused by CCl_4, is observed in many human hepatopathies that cause hepatic fibrosis.[40,59] In this study, mice were randomly divided into 4 groups (n = 6 per group): control group (CTL group), model group (CCl_4 group), low-dose COS group (LC group), and high-dose COS group (HC group). Mice were treated according to previous methods.[21,22] Briefly, all groups of mice except the CTL group were treated with 20% CCl_4 solution in olive oil twice a week at a dosage of 4 mL kg^{-1} (i.p.) for 4 weeks to construct a hepatic fibrosis model, while mice in CTL group received the same volume of olive oil (i.p.). Mice in the LC and HC groups were then additionally gavaged with 100 mg/kg COS and 250 mg/kg COS once a day for 4 weeks, respectively.

Influence evaluation and scheme exploration of Phe and Tyr

Mice were randomly divided into 7 groups (n = 6 per group). The CTL and CCl_4 groups were treated as described above. Mice in the COS group were gavaged with COS (250 mg/kg/day) once a day for 4 weeks. Mice in the Phe and Tyr supplementation group (AA group) received a habitual diet supplemented with 2% Tyr and 2% Phe. Besides, the mTORC1 inhibitor (rapamycin, RAP) and activator (MHY1485, MHY) were applied. Mice in the RAP-treated group (RAP group) received RAP at a dose of 2.0 mg/kg (i.p., every other day) for 4 weeks,[60] while those in the MHY group received MHY (i.p.) at a dose of 10 mg/kg during the last 10 days of the experiment, prior to being sacrificed.[61] Additionally, 4 composite treatment groups (AA + CCl_4, AA + CCl_4+COS, AA + CCl_4+RAP, and AA + CCl_4+COS+MHY groups) were set up, for which the chemicals used were in accordance with the corresponding single component administration groups.

Cell culture and treatment

In vitro experiments were conducted using a hepatic cell line (L-02 cells) and HSCs (LX-2 cells). These cells have been characterized at the cell bank by DNA fingerprinting analysis using short tandem repeat markers, and were tested for mycoplasma contamination by quantitative real-time PCR (qRT-PCR) assay. L-02 cells and LX-2 cells were cultured in RPMI 1640 medium (Gibco, USA) and DMEM medium (Gibco, USA)

supplemented with 10% fetal bovine serum (FBS) (Biological Industries, Beit Haemek, Israel) at 37°C in an environment containing 5% carbon dioxide, respectively.

Induction of hepatocyte damage by H_2O_2

L-02 cells (5×10^4 cells/well) were seeded in 12-well plates. After 24 h of incubation, they were stimulated with or without 1 mM H_2O_2 or COS (LC group 100 μg/mL, HC group 200 μg/mL) for 24 h. The RPMI 1640 medium without FBS supplemented with Phe and Tyr (Tyr 20 μg/mL, Phe 15 μg/mL; 1×) was replaced for 12 h prior to determination via high-performance liquid chromatography (HPLC). Phe and Tyr were added according to the formulations provided by Sigma-Aldrich.

Treatment with Phe and Tyr

L-02 cells or LX-2 cells (1×10^5 cells/well) were seeded in a 6-well plate. The cells were incubated with different combinations of Phe and Tyr (AA group) for 24 h, which were prepared according to the formulations provided by Sigma-Aldrich, to explore the cascade effects on cells and further to determine the concentration causing cell damage for subsequent experiments. Moreover, cells were simultaneously incubated with Phe and Tyr at determined concentrations and with or without COS (LC group 100 μg/mL, HC group 200 μg/mL) for 24 h. For treatment with mTORC1 inhibitor and activator, the inhibitor RAP (25 nM, RAP group) and activator MHY (10 μM, MHY group) were added to the medium for 24 and 4 h, respectively.[62,63]

METHOD DETAILS

Mitochondrial membrane potential analysis

Cells were stained with a JC-1 fluorescence probe for 30 min, according to the manufacturer's instructions. The monomers (green, Ex/Em = 490/527 nm) and aggregates (red, Ex/Em = 490/590 nm) were observed via confocal laser scanning microscopy (Leica AG, Wetzlar, Germany).

Determination of aromatic amino acid levels by HPLC

The serum was mixed with 10% trichloroacetic acid in equal volume, after standing at room temperature for 1 h, centrifuge at 15,000 rpm for 30 min. Then the supernatant was obtained for detection. The levels of serum or medium amino acid in mice were examined by HPLC (Agilent 1100, USA) using calibration curve constructed by plotting values of the area under the peak versus obtained concentration. HPLC was performed using a variable wavelength detector (VWD) with detection wavelength 338 nm and Agilent Hypersil ODS column (4.60*250 mm, 5 μm), column temperature at 40°C. The buffer system composed of mobile phase A (27.6 mmol/L sodium acetate: triethylamine: tetrahydrofuran = 500: 0.11: 2.5, pH = 7.2) and mobile phase B (80.9 mmol/L sodium acetate: methanol: acetonitrile = 1: 2: 2, pH = 7.2). Amino acid was separated using the following gradient elution: 0 min, 8% B; 17 min, 50% B; 20.1 min, 100% B; 24 min, 0% B. The velocity of flow mobile phase was 1.0 mL/min.

Serum metabolite profiling

The serum samples with 100 μL were supplemented with 400 μL methanol (pre-cooled at −20°C), then the mixture was vortexed for 60 s and centrifuged at 4°C for 10 min at 12000 rpm, and then transfer all supernatant from each sample into another 2 mL centrifuge tube. Samples were concentrated to dry in vacuum. Dissolve samples with 150 μL 2-chlorobenzalanine (4 ppm) 80% methanol solution, and the supernatant was filtered through 0.22 μm membrane to obtain the prepared samples for LC-MS. Then take 20 μL from each sample to the quality control (QC) samples and use the rest of the samples for LC-MS.

Chromatographic separation was accomplished in a Thermo Ultimate 3000 system equipped with an ACQUITY UPLC HSS T3 (150 × 2.1 mm, 1.8 μm, Waters) column maintained at 40°C. The temperature of the autosampler was 8°C. Gradient elution of analytes was carried out with 0.1% formic acid in water (C) and 0.1% formic acid in acetonitrile (D) or 5 mM ammonium formate in water (A) and acetonitrile (B) at a flow rate of 0.25 mL/min. Injection of 2 μL of each sample was done after equilibration. An increasing linear gradient of solvent B (v/v) was used as follows: 0–1 min, 2% B/D; 1–9 min, 2%–50% B/D; 9–12 min, 50%–98% B/D; 12~13.5 min, 98% B/D; 13.5–14 min, 98%–2% B/D; 14–20 min, 2% D-positive model (14–17 min, 2% B-negative model).

The ESI-MSn experiments were executed on the Thermo Q Exactive mass spectrometer with the spray voltage of 3.5 kV and −2.5 kV in positive and negative modes, respectively. Sheath gas and auxiliary gas were set at 30 and 10 arbitrary units, respectively. The capillary temperature was 325°C. The analyzer scanned over a mass range of m/z 81–1000 for full scan at a mass resolution of 70,000. Data dependent acquisition (DDA) MS/MS experiments were performed with HCD scan. The normalized collision energy was 30 eV. Dynamic exclusion was implemented to remove some unnecessary information in MS/MS spectra.

In univariate statistical comparisons, Chi-square test was used for categorical variables, Student's t test or ANOVA for normal continuous variables and Wilcoxon signed rank test or Kruskal Wallis test for not normal continuous variables. Spearman was used for not normally distributed variables correlations. Metabolome values were transformed to log2 adding 0.01 to avoid indetermination. Differential metabolite satisfying the conditions (VIP>1.0 and p < 0.05 in ANOVA) were used as potential biomarkers in the Venn diagram analysis. Metpa database, Kyoto Encyclopedia of Genes and Genomes (KEGG) database and hypergeometric test were used for enrichment analysis. This analysis was performed by querying different databases including Human Metabolome Database (HMDB) (http://www.hmdb.ca), Metlin

(http://metlin.scripps.edu), massbank (http://www.massbank.jp/), LipidMaps (http://www.lipidmaps.org) and mzclound (https://www.mzcloud.org). All tables and plots, including heatmaps and correlation network were generated using 3.6.1 R packages.

16S rRNA gene pyrosequencing and analysis

The CTAB/SDS method was used to extract the total genome DNA in samples. DNA concentration and purity were monitored on 1% agarose gels. According to the concentration, DNA was diluted to 1 ng/µL with sterile water. 16S rRNA genes in distinct regions (V3-V4) were amplified with specific primer (341F- 805R) and barcodes. All PCR mixtures contained 15 µL of Phusion High-Fidelity PCR Master Mix (New England Biolabs), 0.2 µM of each primer and 10 ng target DNA, and cycling conditions consisted of a first denaturation step at 98°C for 1 min, followed by 30 cycles at 98°C (10 s), 50°C (30 s) and 72°C (30 s) and a final 5 min extension at 72°C. Mix an equal volume of 1 X loading buffer (contained SYB green) with PCR products and perform electrophoresis on 2% agarose gel for DNA detection. The PCR products were mixed in equal proportions, and then Qiagen Gel Extraction Kit (Qiagen, Germany) was used to purify the mixed PCR product. Following manufacturer's recommendations, sequencing libraries were generated with NEBNext Ultra IIDNA Library Prep Kit (Cat No. E7645). The library quality was evaluated on the Qubit@ 2.0 Fluorometer (Thermo Scientific) and Agilent Bioanalyzer 2100 system. Finally, the library was sequenced on an Illumina NovaSeq platform and 250 bp paired-end reads were generated.

For the Effective Tags obtained previously, denoise was performed with DADA2 or deblur module in the QIIME2 software (Version QIIME2-202006) to obtain initial ASVs (Amplicon Sequence Variants) (default: DADA2), and then ASVs with abundance less than 5 were filtered out. The absolute abundance of ASVs was normalized using a standard of sequence number corresponding to the sample with the least sequences. Subsequent analysis of alpha diversity and beta diversity were all performed based on the output normalized data. Partial least squares-discriminant analysis (PLS-DA) was used to assess the variation between experimental groups (beta diversity). The LEfSe software (Version 1.0) was used to do LEfSe analysis (LDA score threshold: 2) so as to find out the biomarkers. Predictive functional outputs (KEGG Orthologs (KOs) pathway abundance) was completed by using the PICRUSt2 plugin for QIIME2. The t-test and PLS-DA projection were conducted in R (V.3.1.3), $p < 0.05$ was considered significant.

Histopathological and immunohistochemical analysis

Liver tissue samples were fixed for 24 h in 4% formalin solution in phosphate buffer, embedded in paraffin, and sliced into 5 µm paraffin tissue slices, which were stained with hematoxylin and eosin and Sirius red. Subsequently, positive areas were quantified using ImageJ software (National Institutes of Health, Bethesda, MD, USA).

Western blotting analysis

Proteins were extracted using a protein extraction buffer and then separated by SDS-PAGE. Afterward, the gel was transferred to polyvinylidene fluoride membranes, which were then probed with primary antibodies and secondary antibodies. Thereafter, the target protein blots were visualized using enhanced chemiluminescence reagents (Thermo Fisher Scientific, MA, USA). Samples from 6 mice were mixed in pairs, and then the protein levels were determined.

Quantitative real-time PCR (qRT-PCR) assay

Total RNA was isolated using TRIzol, and then 1 µg was used to synthesize cDNA using 5× All-In-One RT Master Mix kit. Next, qRT-PCR was performed in a reaction containing 200 ng cDNA, SYBR Green Master Mix, and 5 nM primer pair (Table 1) under the following cycling conditions: 40 cycles at 95°C for 1 s and 60°C for 20 s. The relative levels of mRNA were determined (CFX96 Touch; Bio-Rad Laboratories, Hercules, CA, USA) and calculated using the 2-ΔΔCt method.

QUANTIFICATION AND STATISTICAL ANALYSIS

All data are presented as means with their standard deviations. The results were assessed via one-way analysis of variance with Tukey's post hoc tests, and the normality and homogeneity of the data were evaluated using the Shapiro–Wilk test. Analysis items with $p < 0.05$ were considered statistically significant. The statistical analyses were performed using GraphPad Prism version 8.0.1 (GraphPad Software Inc., San Diego, CA, USA) and SPSS version 21.0 (SPSS Inc., Chicago, IL, USA).